

DRAFT: June 13, 2014

The Orion Fingers: Near-IR Adaptive Optics Imaging of an Explosive Protostellar Outflow

John Bally¹, Adam Ginsburg²,

¹ Department of Astrophysical and Planetary Sciences,
University of Colorado, UCB 389,
Boulder, CO 80309

John.Bally@colorado.edu

² ESO Headquarters Karl-Schwarzschild-Str. 2 85748 Garching bei Mnchen Germany

Adam.Ginsburg@eso.org

ABSTRACT

We present new narrow-band H₂, [Fe II], and broad-band K_s images of the Orion OMC1 outflow obtained with the Gemini South multi-conjugate adaptive optics (AO) system and near-infrared imager GSAOI. These images reach the diffraction limit of the 8-meter telescope at 2 μ m of about 0.05''. Comparison with previous AO-assisted observations of sub-fields with the Gemini North telescope between 2007 to 2009 and ground-based observations going back to 1999 enable measurements of proper motions of H₂ and [Fe II] features with unprecedented precision in portions of the outflow. Several sub-arcsecond H₂ features and many [Fe II] ‘fingertips’ on the projected outskirts of the flow show proper motions of \sim 300 km s⁻¹. The propagation of compact knots (‘bullets’) as far as 140'' from their ejection sites through the dense OMC1 core sets a lower bound on their densities. The density, mass, and energy constraints are consistent with the disruption of dense circumstellar disks within a few AU of massive stars during a final multi-body dynamic encounter that ejected the BN object and radio source I from the OMC1 about 500 years ago.

Orion is frequently, and appropriately, used as a template for understanding other massive star forming regions. These new data provide excellent evidence for shock-heated, megaKelvin gas generating H₂ emission in interaction regions with a molecular cloud. Such interaction zones are likely to be a common feature in high-mass-star forming regions and will likely dominated the H₂ emission from such regions.

Subject headings: ISM: - molecular clouds – ISM: - shocks, outflows ISM: individual – Orion Nebula, OMC1 stars: formation –

1. Introduction

The BN/KL region behind the Orion Nebula, located at a distance of about 414 pc (Menten et al. 2007) contains a spectacular, wide opening-angle, arcminute-scale outflow emerging from the OMC1 cloud core. The flow is traced by the millimeter and sub-millimeter emission lines of molecules such as CO, CS, SO, SO₂, and HCN that exhibit broad ($> 100 \text{ km s}^{-1}$) emission line wings (Kwan & Scoville 1976; Wiseman & Ho 1996; Furuya & Shinnaga 2009), high-velocity OH, H₂O, and SiO maser emission (Genzel et al. 1981; Greenhill et al. 1998), and bright shock-excited ‘fingers’ of H₂ and ‘fingertips’ of 1.64 μm [Fe II] emission (Allen & Burton 1993; Bally et al. 2011). The OMC1 outflow with a southeast (red-shifted) - northwest (blue-shifted) axis contains at least 8 M_⊙ of accelerated gas with a median velocity of about 20 km s⁻¹. Interferometric CO images, H₂O and the 18 km s⁻¹ SiO masers, and dense-gas tracers such as thermal SiO reveal a smaller (8'' long) and younger (~ 200 year old) outflow along a northeast-southwest axis emerging from radio source I orthogonal to the arc-minute-scale CO outflow (Beuther & Nissen 2008; Plambeck et al. 2009). The momentum and kinetic energy content of these flows is at least 160 M_⊙ km s⁻¹ and 4×10^{46} ergs (Snell et al. 1984) to 4×10^{47} ergs (Kwan & Scoville 1976). Zapata et al. (2009) presented a CO J = 2–1 interferometric study and found a dynamic age of about 500 years for the larger OMC1 outflow. They noted its impulsive nature, that its structure is different from accretion-disk powered flows, and that it originated several arc-seconds north of the OMC1 hot-core.

The OMC1 outflow contains a complex of shocks which may indicated an explosive origin. High precision astrometric measurements have shown that the three brightest radio-emitting stars in OMC1, sources BN, I, and possibly source n, have proper motions of 25, 15, and 26 km s⁻¹ away from a region less than 500 AU in diameter from which they were ejected about 500 years ago (Rodriguez et al. 2005; Gomez et al. 2005; 2008). Bally et al. (2011) and Goddi et al. (2011) proposed that the explosion was triggered by the dynamical rearrangement of a nonhierarchical system of massive stars in OMC1 which resulted in the formation of a compact, massive binary (most likely source I) and the ejection of both BN, source I, and possibly source n. Proper motion measurements show that the fastest components in the OMC1 fingers have a dynamic age of about 500 years (Bally et al. 2011), consistent with this scenario.

On the other hand, Tan (2004) proposed that the decay occurred about 4,000 years ago in the Trapezium cluster located in the center of the Orion Nebula and that the OMC1 explosion

was triggered by the close passage of the BN object through the OMC1 core. Although this scenario requires a highly unlikely close encounter of BN with source I, Chatterjee & Tan (2012) show that the the parameters of the Trapezium and BN are compatible with this scenario.

Though rare, the explosive outflow morphology of the OMC1 outflow is not unique; other likely examples (Bally et al. 2011). However, Orion BN/KL is the nearest and least obscured, and thus most accessible for high-resolution studies. Here, we present 0.06 to 0.1 arc second resolution images of the entire OMC1 outflow complex in the $1.64\ \mu\text{m}$ [Fe II] and $2.12\ \mu\text{m}$ H₂ narrowband filters and a broad-band K_s obtained with adaptive optics (AO) on the Gemini South 8 meter telescope. This data is combined with older AO-assisted observations obtained on Gemini North and natural seeing-limited images acquired with a variety of other telescope to measure new proper motions.

2. Observations

2.1. Gemini South GEMS

The Gemini Multi-conjugate adaptive optics System (GeMS) at the Gemini South telescope in Cerro Pachon is the first and only sodium-based multi-Laser Guide Star (LGS) adaptive optics system (Rigaut et al. 2014, 2012; Neichel et al. 2014, 2013; d'Orgeville et al. 2012). GeMS works with a LGS constellation of 5-spots: 4 of the LGS spots are at the corners of a $60''$ square, with the 5-th positioned in the center. The Adaptive Optics (AO) bench called Canopus is mounted on one of the f/16 Cassegrain ports. Gemini South Adaptive Optics Imager (GSAOI) is a wide-field ($85''$ by $85''$ field of view) camera designed to work at the diffraction limit of the 8-meter telescope in the near-infrared. Three $85''$ fields were observed in OMC1 between 30 December 2012 and 28 February 2013 using GSAOI. Observations of each field were obtained though 1% bandpass narrow-band filters centered on the $1.644\ \mu\text{m}$ [FeII] and $2.122\ \mu\text{m}$ H₂ emission lines and the broad-band K_s filter. The corrected images have FWHM diameters of $0.06''$ to $0.1''$, providing the highest angular resolution images of the BN/KL outflow ever obtained in the near-IR.

Each field was imaged in each filter with a 5 point dither pattern to fill-in gaps between the four 2048 by 2048 pixel arrays in GSAOI. In the two narrow band filters, exposure times of 30 seconds per image were used; exposure times were 10 seconds per frame were used in the broad-band filter.

Exposure times were 43.4 seconds per exposure for H₂, 43.0 for [Fe II], and 15.0 for K_s. 10 exposures were taken in each filter for a total of 430s on-source in the narrow-band filters

and 150s in the continuum filter.

Data were processed with the Gemini pipeline. However, additional astrometric corrections were required. Individual exposures were first registered to the Muench et al. (2002) catalog sources to acquire a world coordinate system with RMS pointing error $\sim 0.1''$. A new catalog of relative star positions was generated from a preliminary aligned and co-added stack of images and used to derive a distortion map for GSAOI. The individual distortion corrected images were re-aligned and co-added to form the final mosaic in each filter.

2.2. Gemini North Altair

The Gemini North 8 meter telescope was used to observe the OMC1 region using the Altair AO system with the NIRI near-IR camera through 1% narrow-band [Fe II], H₂, and broad-band K_s filters. NIRI was used in a configuration which delivers a 40'' field of view. In the narrow-band filters, a dithered set of five to 10 30 second duration exposures were obtained. A similar set of 10 second exposures were acquired in the K_s filter. In 2007, only the ‘H₂ fingers’ region was observed as part of the commissioning of the Altair AO system using the NIRI camera. During 2008 and 2009, we intended to image a 3×4 point grid to cover the full extent of the BN/KL outflow. However, on 5 and 8 fields were actually observed in 2008 and 2009, respectively. Only the ‘H₂ fingers’ field was observed during each of the three years. A summary of the observations is given in Table 1. The angular resolution of the NIRI images ranges from 0.1 to 0.2''.

AO images were obtained with Gemini North on MJD 54165, MJD 54753, and MJD 55138 between 2007 and 2009, and Gemini South on MJD 56323. In the analysis presented here, the NIRI images were registered to the final GSAOI mosaic using IRAF tasks GEOMAP and GEOTRAN applied to unsaturated field stars. Proper motions were determined by marking the photocenters of features on the multi-epoch images. Images of the OMC1 outflow obtained with the Subaru 8 meter telescope on MJD = 51484 in 1999 (Kaifu et al. 2000), the Apache Point Observatory 3.5 meter on MJD = 53331 in 2004 (Bally et al. 2011) are also used for analysis. These observations span an interval of 4,839 days.

3. Results

The 2013 epoch GSAOI images presented here reach the near-IR diffraction limit of an 8-meter telescope and provide sharpest views obtained thus far of the entire OMC1 BN/KL outflow. The image (Figure 1) shows dozens of H₂ fingers tipped with [Fe II] emission

extending from about $30''$ to $140''$ from the OMC1 core. For the analysis of dynamic ages for various features, we assume that all features originated from J2000 = 05:35:14.350, -05:22:28.50, the suspected location from which the BN object and radio source I were ejected about 500 years ago (Gómez et al. 2008). The two brightest [Fe II] bow shocks correspond to the Herbig-Haro objects HH 201 and HH 210 located $60''$ northwest and $113''$ north of OMC1 (Gull et al. 1973; Münch & Taylor 1974; Canto et al. 1980; Axon & Taylor 1984). These shocks are visible on ground-based and Hubble Space Telescope images in [O I], H α , [N II] and S II. However, they only exhibit very faint H $_2$ emission (Graham et al. 2003), indicating that they lie in the mostly atomic photon-dominated region (PDR) located between the Orion Nebula's ionization front and the background molecular cloud. The most prominent H $_2$ finger consist of multiple [Fe II] finger-tips trailed by H $_2$ wakes, has an orientation of PA ~ 340 to 345° , and can be traced from about $50''$ to about $135''$ from the ejection center. This wake consists of at least a dozen nested H $_2$ bow shocks tipped with [Fe II] emission regions. The brighter [Fe II] knots corresponding to HH 205 through 209 are associated with the tips of a train of H $_2$ wakes propagating toward position angle (PA) ~ 340 to 350° . These HH objects are associated with the PA ~ 340 to 345° finger.

More than 120 distinct wakes are visible in the $2.12\ \mu\text{m}$ H $_2$ images presented here. The H $_2$ wakes exhibit nearly parallel walls, large proper motions along their axes (Bally et al. 2011). Figure 2 shows a median filtered version of the 2013 GSAOI mosaic. This high-pass filtered image was created by convolving the original images with a 51 pixel kernel ($1''$; each pixel is $0.02''$ on a side) using IRAF function MEDIAN, and subtracting the the result from the original image. Vectors were drawn from the suspected ejection site of radio sources BN and source I (the coordinates are given above) to each H $_2$ or [Fe II] fingertip. The H $_2$ emission becomes too contused within $\sim 30''$ of the suspected ejection location due to the complex of multiple overlapping features. The natural seeing limited 1999 epoch Subaru image from Kaifu et al. (2000) and the 2005 epoch image from Bally et al. (2011) were used to trace additional H $_2$ fingers beyond the boundaries of the GSAOI image. The dashed vector near the top marks a chain of H $_2$ knots and bow shocks with proper motions nearly orthogonal to the northern fingers suspected to trace a background flow originating east of the present field. This flow is also seen faintly in visual wavelength images and exhibits large proper motions.

While the fingertips tend to be faint or invisible in H $_2$, most of the the [Fe II] emission in the BN/KL outflow originates from the fingertips. Dozens of wake-tips (fingertips) are visible in the $1.64\ \mu\text{m}$ [Fe II] line. The two cyan vectors point to the two brightest [Fe II] features, HH 201 and 210. These fingertips are very faint in H $_2$. Figure 4 shows a color version of the ‘H $_2$ fingers’ region in 2013 from GSAOI.

In the northwestern part of the flow, the H₂ wakes range in diameter from 2 to 8'' (7×10^{14} to 3×10^{15} cm) with limb brightened rims less than 1'' (< 3×10^{14} cm) wide (Figure 3). The half dozen major finger clusters in the northwest are up to 60'' (~ 0.1 pc) long. The wakes in the inner part of the flow are narrower, tend to be shorter, and are more numerous resulting in a high degree of overlap along the line-of-sight. The H₂ emission tends to be fainter or disappears near the wake-tips where it is replaced by [Fe II] emission. [Fe II] emission is only found near the fingertips, some of which show evidence for fragmentation.

3.1. Proper Motions of Selected Knots

Previous analyses of multi-epoch ground-based images have shown that the overall expansion pattern of the BN/KL outflow is a ‘Hubble flow’ with the proper motions being approximately proportional to the projected distance from OMC1 (Jones & Walker 1985; Lee & Burton 2000; Bally et al. 2011).

(Kaifu et al. 2000)

Figure 3 shows a difference

Comparison of sub-fields with 2007, 2008, 2009 Gemini North NIRI images show large proper motions of [Fe II]-dominated fingertips and slowly expanding H₂wakes (the H₂ fingers). However, there are several compact, fast moving H₂ knots which have sub-arc-second to arc-second diameters. The most reliable proper motions were measured in the ‘H₂ fingers’ field where we have AO-assisted images from both 2013 and 2007 separated by 2,125 days. Figure 4 shows a color composite image of this field. and 6 show the differences between the H₂ and [Fe II] images taken in 2013 and 2007.

A difference image formed by subtracting a de-distorted, intensity matched, and registered 2013 GSAOI image from the 2007 NIRI image (Figures 5) shows that the H₂ wakes are spreading with velocities ranging from 20 to 80 km s⁻¹.

The most prominent high-velocity compact clump (HVCC - Figure 2) exhibits a proper motion of 350 ± 20 km s⁻¹ and over the 6 year (1.85×10^8 sec.) interval between the Gemini North and South images in 2007 and 2013. This HVCC is located at projected distance of 100'' from source I and 97'' from the suspected location of the dynamic ejection of source I and BN about 500 years ago. Assuming no deceleration, the dynamic age of this knot is $t_{dyn} = d/V \approx 350 \pm 30$ years.

This HVCC has undergone considerable transverse spreading over the past 6 years indicating that it may be experiencing photometric variations or significant deceleration.

Several less-prominent HVCCs exhibit motions of 200 - 300 km s⁻¹. Measured motions of a sample (subset) of fingertips, H₂ wakes, and compact, fast knots are given in Table 1.

While the H₂ fingers show fast > 100 km/s) forward motion, they spread at less than 50 km s⁻¹ orthogonal to their orientation, consistent with their large length-to-width ratios. The proper motions of the northwestern fingertips as well as those located west of the OMC1 core range from 200 to 400 km s⁻¹ with a pattern of increasing velocity with increasing distance from OMC1. They have dynamic ages consistent with ejection between 450 and 600 years ago.

Comparison of HST images in [OI] and [SII] taken on MJD 50170 show that the HVCC is located a few arc second south of HH 207.

HH 205, 206, and 207 trace the visual counterpart of the PA \sim 340 to 345° finger. The [Fe II] counterpart of HH 207 exhibits a prompter motion of 214 km s⁻¹.

The side jet is a visual HH object with large motions.

d132-042 (Smith et al. 2005) has an [Fe II] micro-jet.

3.2. Constraints on the ejection mechanism

Assuming the ejection occurred \sim 500 years ago at approximately the location of the BN/KL infrared nebula, the most distant knots to the northwest provide constraints on the ejecta properties. These knots have traveled \sim 0.28 pc in projection in \sim 500 years. Thus, the time-averaged velocities must be greater than \sim 550 km s⁻¹. For an explosive origin, the fingertips proper motions should decrease linearly with decreasing distance from the launch region. The northern and northwestern [Fe II] fingertips show motions of \sim 400 km s⁻¹. While a few H₂ features have proper motions between 300 and 350 km s⁻¹, most show lower velocities, especially closer to the OMC1 core. Because the faster motions are at least 20% slower than expected for a 500 year-old explosion, the ejecta may have suffered some deceleration.

Several dozen [Fe II] knots and HVCCs seen in H₂ have diameters of about 1 " (\sim 400 AU) or less and are located more than 100" from their ejection site. Such clumps could have been powered by a faster wind that had experienced instabilities causing it to break-up into a multitude of finger-shaped protrusions McCaughrean & Mac Low (1997). Rayleigh-Taylor instabilities can produce fingers of fast ejecta surrounded by slower clumps of dense gas if the wind velocity increases with time on a time scale shorter than the mean crossing time, or if the wind runs into a stationary medium with a density profile which decreases faster

than r^{-2} . However, neither an accelerating wind, nor a wind that runs down a steep density gradient would naturally explain the approximately Hubble-flow type behavior with V_{max} increasing linearly with increasing projected distance from the source that is exhibited by the fasted ejecta (Bally et al. 2011). Nor do wind models easily form compact clumps near the fingertips.

Alternatively, the wakes and fingers may be driven by compact, high-density ejecta (bullets or HVCCs) originating within a few AU of the massive stars in OMC1. In this model, momentum conservation sets a minimum constraint on the ejecta density because they have move through the dense gas in the Orion molecular cloud. Momentum conservation indicates that such knots must be denser than the environment into which they are moving. A spherical clump 170 AU in diameter that moved more than 0.2 pc into a medium with density $n(H_2) = 10^4 \text{ cm}^{-3}$ must have an H_2 density $> 10^6 \text{ cm}^{-3}$ in order to preserves at least half of its initial ejection velocity. If the clump is expanding with an internal sound speed c_s , the Mach angle is given my $M \sim c_s/2V$. Using the observed sized of compact [Fe II] and H_2 knots and a distance of greater than 0.2 pc from the ejection site implies $c_s < 0.6 \text{ km s}^{-1}$. A 170 AU diameter sphere with density $> 10^6 \text{ cm}^{-3}$ has a mass $> 10^{29}$ grams.

The properties of the H_2 wakes provide constrains on the density of the ambient medium into which the suspected HVCCs are moving. The wakes have widths that are an order-of-magnitude wider than the HVCCs and [Fe II] fingertips ($2''$ to $10''$ with most being near the lower-end of this range). The formation of such wide wakes requires that the post-shock layer forming between the forward shocks and a high-velocity, dense clump (or working surface of a jet) have a cooling length larger than the clump diameter or jet (Blondin et al. 1990). The post-shock temperature immediately behind a shock is given by $T_{ps} = 3\mu V_s^2/16k$ where $V_s \sim 300$ to 500 km s^{-1} is the forward shock speed. The cooling distance is then given by $d_{cool} = V_s t_{cool}/4 = 9\mu V_s^3/64n_0\Lambda(T_{ps})$ where μ is the mean molecular weight of the pre-shocked gas particles and $\Lambda(T_{ps})$ is the cooling function (Blondin et al. 1990). Numerical studies of the cooling function give $d_{cool} \approx 4.5 \times 10^{16} V_{100}^{4.0}/n_0$ where V_{100} is the shock velocity in units of 100 km s^{-1} and n_0 is the pre-shock particle density. Modern numerical calculations give $d_{cool} \approx 5.5 \times 10^{17} V_{100}^{4.4}/n_0$ for $80 \text{ km s}^{-1} < V_s < 1,200 \text{ km s}^{-1}$ (Draine 2011). Thus, a $V_s = 300 \text{ km s}^{-1}$ shock moving into a density $n_0 = 10^4 \text{ cm}^{-3}$ has a cooling length $L_{cool} \sim 7 \times 10^{15} \text{ cm}$ (470 AU). Thus, for densities between 10^3 and 10^4 , cooling lengths will correspond to 1.1 to $11''$ in the frame of the shock at the distance of Orion, larger than the HVCCs and [Fe II] knots.

For a very dense HVCCs, the hot ($\sim 6 \text{ MK}$) plasma will squirt sideways to produce a wide bow-shaped wake. The sideway expansion into the surrounding medium drives a slower ($V_{side} < 50 \text{ km s}^{-1}$) shock where the observed H_2 emission in the wakes is produced.

In the OMC1 rest frame the 30 to 300 year cooling time corresponds to a wake-length $L_{wake} \sim 3 \times 10^{16}$ to 3×10^{17} cm, comparable to the lengths of fingers in the north and west parts of the OMC1 outflow.

While most fingertips are invisible Doi et al. (2002) measured visual wavelength proper motions for Herbig-Haro (HH) object which protrude into the photon-dominated region behind the Orion Nebula. Two of the brightest [Fe II] features correspond to HH 201 northwest of OMC1 and 210 north of OMC1. citetDoi2002 measured proper motions of 312 to 315 km s⁻¹ for various components of HH 201 and 309 to 425 km s⁻¹ for knots in HH 210. Grosso et al. (2006) detected X-rays from the wake of HH 210, which is the highest proper motion finger in the OMC1 outflow and one of the relatively few visible at visual wavelengths, thereby demonstrating that at least some of the fingers contain hot, X-ray emitting plasma. Additional HH objects are associated with the Orion fingers including HH 205 to 209, and HH 601 to 607 with proper motion velocities ranging from 100 to 300 km s⁻¹ (Doi et al. 2002). All of these features have large negative radial velocities. For example, HH 201 has $V_{LSR} \sim -260$ to -284 km s⁻¹ (Doi et al. 2004).

Predictions for ALMA (dust and gas column density)

Comparison of selected fingers with models from ENZO code (Devin Silvia)

Is there any correlation between the complex structure of OMC1 revealed by SCUBA? First impression is no .. but there is mechanical ‘shadowing’ by the OMC1 ridge: fingers towards NE and SW are shorter; more resistance or more recent ejecta from the young SiO / H₂O flow from source I?

3.3. Other YSOs in the field

The [FeII] bipolar jet, the silhouette disk. These YSOs (possibly other embedded ones), may be impacted by phase ejecta and shocks!

V* V2270 Ori (05 35 15.3937 -05 21 14.112) is driving a bipolar [Fe II] jet. The jet has a measured velocity different of XXX from TripleSpec spectra XXX though we may not want to report that here?

There is a shadowed disk system at 5:35:14.692 -5:22:20.36. It is most evident in the [Fe II] filter, which could be from the Brackett 8 line at 1.64112 μ m.

4. Conclusions

Summary of results:

- Compact high-density knots may be located at finger tips (from propagation constraint).
- Some have reverse shocks that light-them up in H₂ despite $V \gtrsim 200 \text{ km/s} = \zeta$ independent constraint on density.
- Predict that ALMA will see CO wakes, and detect compact knots of hot gas (SiO? HCO+?, high-J CO?) from "bullets"

REFERENCES

- Allen, D. A. & Burton, M. G. 1993, Nature, 363, 54
- Axon, D. J. & Taylor, K. 1984, MNRAS, 207, 241
- Bally, J., Cunningham, N. J., Moeckel, N., Burton, M. G., Smith, N., Frank, A., & Nordlund, A. 2011, ApJ, 727, 113
- Beuther, H. & Nissen, H. D. 2008, ApJ, 679, L121
- Blondin, J. M., Fryxell, B. A., & Konigl, A. 1990, ApJ, 360, 370
- Canto, J., Goudis, C., Johnson, P. G., & Meaburn, J. 1980, A&A, 85, 128
- Chatterjee, S. & Tan, J. C. 2012, ApJ, 754, 152
- Doi, T., O'Dell, C. R., & Hartigan, P. 2002, AJ, 124, 445
- . 2004, AJ, 127, 3456
- d'Orgeville, C. et al. 2012, in Society of Photo-Optical Instrumentation Engineers (SPIE) Conference Series, Vol. 8447, Society of Photo-Optical Instrumentation Engineers (SPIE) Conference Series
- Draine, B. T. 2011, Physics of the Interstellar and Intergalactic Medium
- Furuya, R. S. & Shinnaga, H. 2009, ApJ, 703, 1198
- Genzel, R., Reid, M. J., Moran, J. M., & Downes, D. 1981, ApJ, 244, 884

- Goddi, C., Humphreys, E. M. L., Greenhill, L. J., Chandler, C. J., & Matthews, L. D. 2011, ApJ, 728, 15
- Gómez, L., Rodríguez, L. F., Loinard, L., Lizano, S., Allen, C., Poveda, A., & Menten, K. M. 2008, ApJ, 685, 333
- Graham, M. F., Meaburn, J., & Redman, M. P. 2003, MNRAS, 343, 419
- Greenhill, L. J., Gwinn, C. R., Schwartz, C., Moran, J. M., & Diamond, P. J. 1998, Nature, 396, 650
- Grosso, N., Feigelson, E. D., Getman, K. V., Kastner, J. H., Bally, J., & McCaughrean, M. J. 2006, A&A, 448, L29
- Gull, T. R., Goad, L., Chiu, H.-Y., Maran, S. P., & Hobbs, R. W. 1973, PASP, 85, 526
- Jones, B. F. & Walker, M. F. 1985, AJ, 90, 1320
- Kaifu, N. et al. 2000, PASJ, 52, 1
- Kwan, J. & Scoville, N. 1976, ApJ, 210, L39
- Lee, J.-K. & Burton, M. G. 2000, MNRAS, 315, 11
- McCaughrean, M. J. & Mac Low, M.-M. 1997, AJ, 113, 391
- Menten, K. M., Reid, M. J., Forbrich, J., & Brunthaler, A. 2007, A&A, 474, 515
- Muench, A. A., Lada, E. A., Lada, C. J., & Alves, J. 2002, ApJ, 573, 366
- Münch, G. & Taylor, K. 1974, ApJ, 192, L93
- Neichel, B. et al. 2014, MNRAS, 440, 1002
- Neichel, B. et al. 2013, in Proceedings of the Third AO4ELT Conference, ed. S. Esposito & L. Fini
- Plambeck, R. L. et al. 2009, ApJ, 704, L25
- Rigaut, F. et al. 2012, in Society of Photo-Optical Instrumentation Engineers (SPIE) Conference Series, Vol. 8447, Society of Photo-Optical Instrumentation Engineers (SPIE) Conference Series
- Rigaut, F. et al. 2014, MNRAS, 437, 2361

Snell, R. L., Scoville, N. Z., Sanders, D. B., & Erickson, N. R. 1984, ApJ, 284, 176

Tan, J. C. 2004, ApJ, 607, L47

Wiseman, J. J. & Ho, P. T. P. 1996, Nature, 382, 139

Zapata, L. A., Schmid-Burgk, J., Ho, P. T. P., Rodríguez, L. F., & Menten, K. M. 2009, ApJ, 704, L45

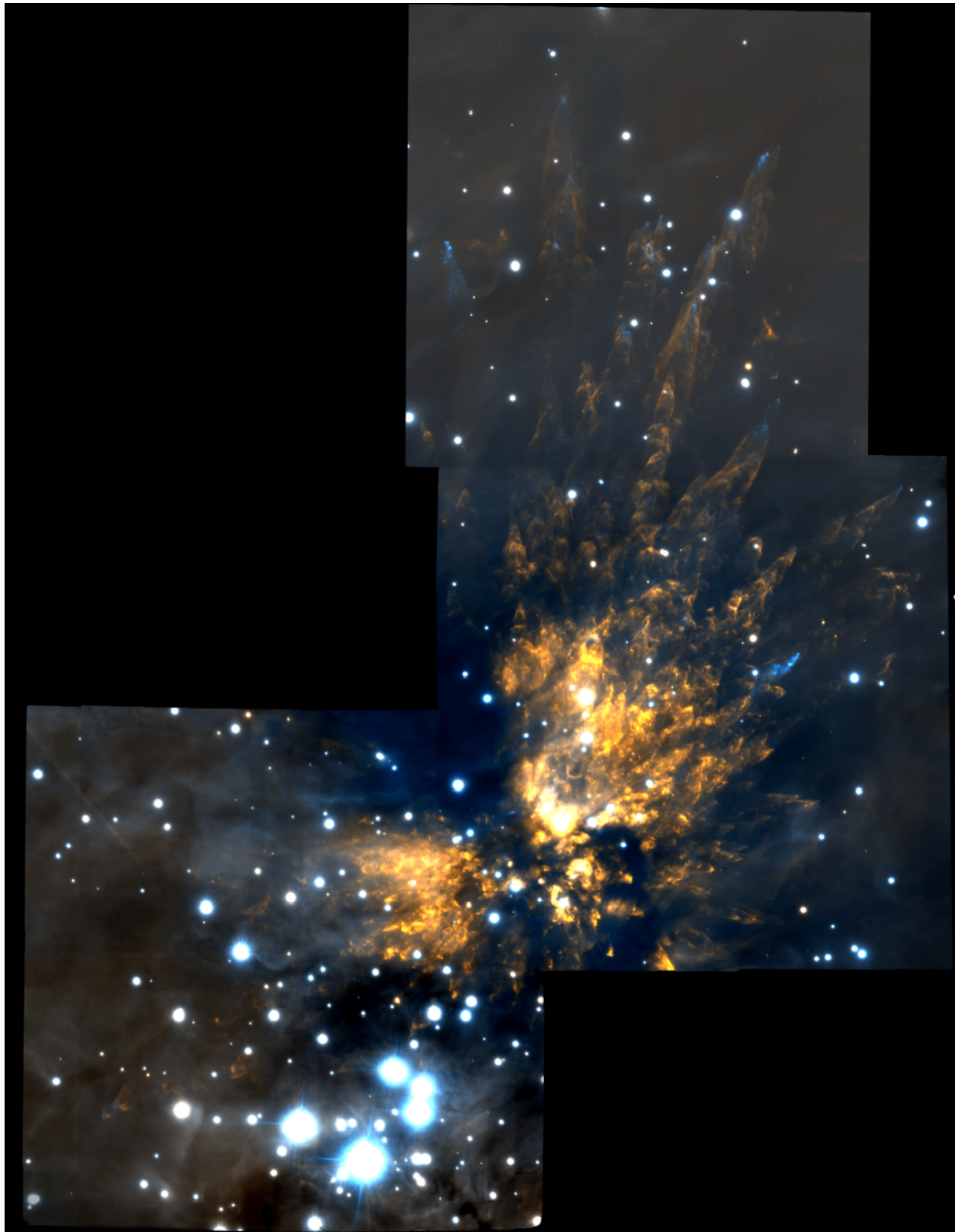


Fig. 1.— A wide-field image showing the OMC1 outflow in H₂ (red) and [Fe II] (cyan).

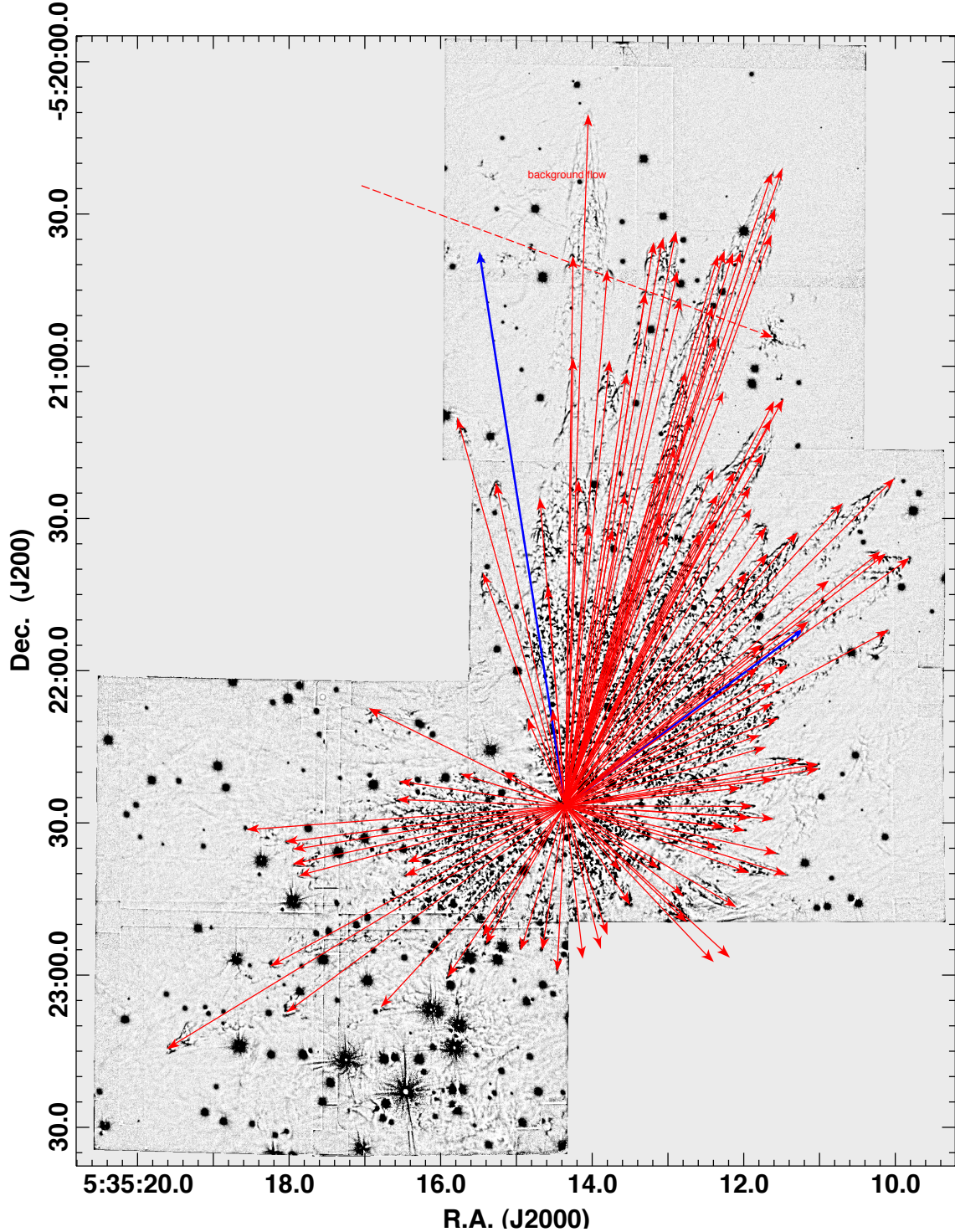


Fig. 2.— The outer system of fingers (vectors) in the $2.122 \mu\text{m}$ H₂ GSAOI image. The dashed vector shows the background flow whose motions are towards the west. The background image has been median filtered as described in the text.

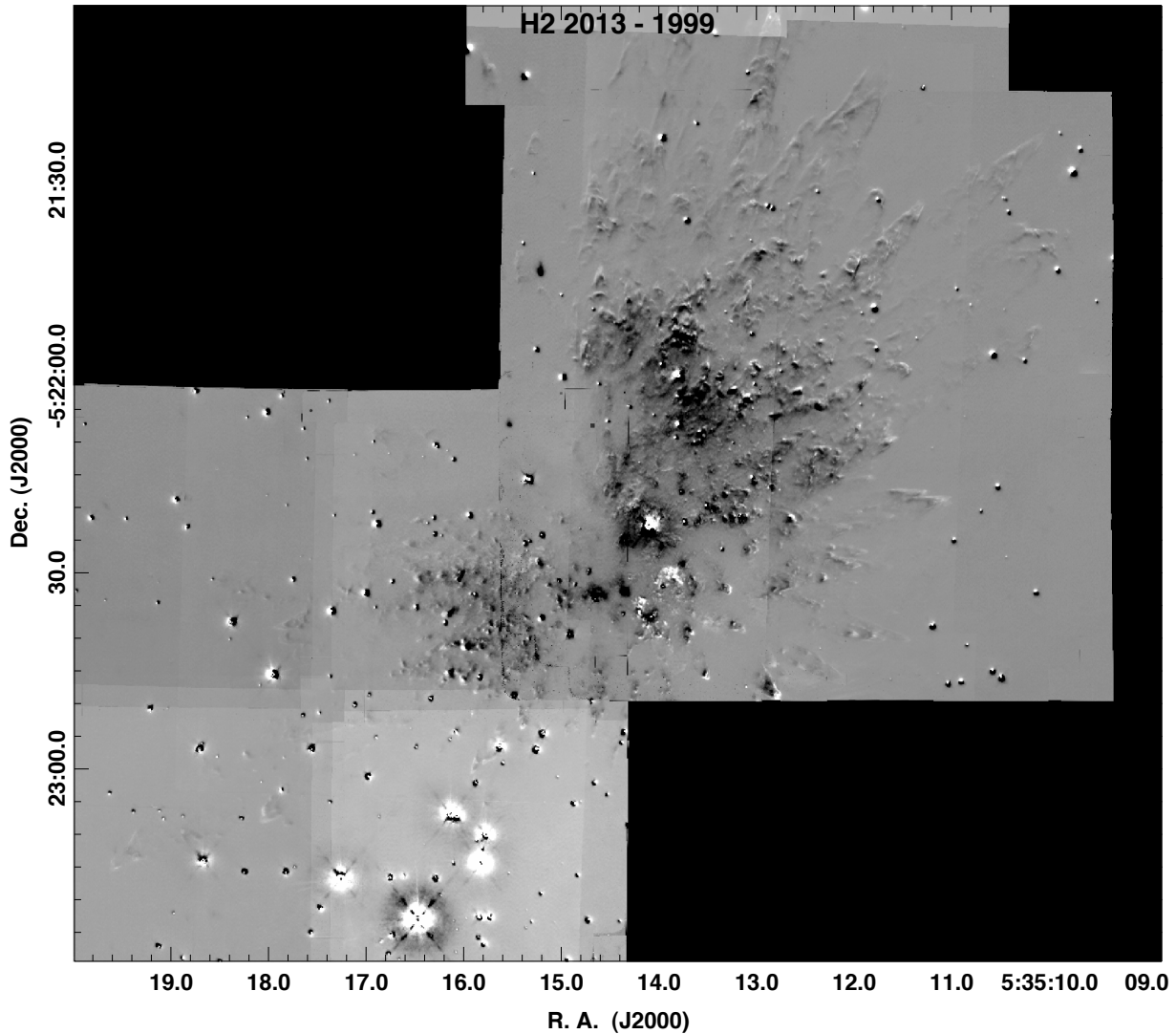


Fig. 3.— A $2.122 \mu\text{m}$ H_2 difference image showing proper motions in the field imaged by Kaifu et al. (1999) with the Subaru telescope in 1999. The images shows the difference between 2013 and 1999 epoch data. Residual distortion corrections result in imperfect registration.

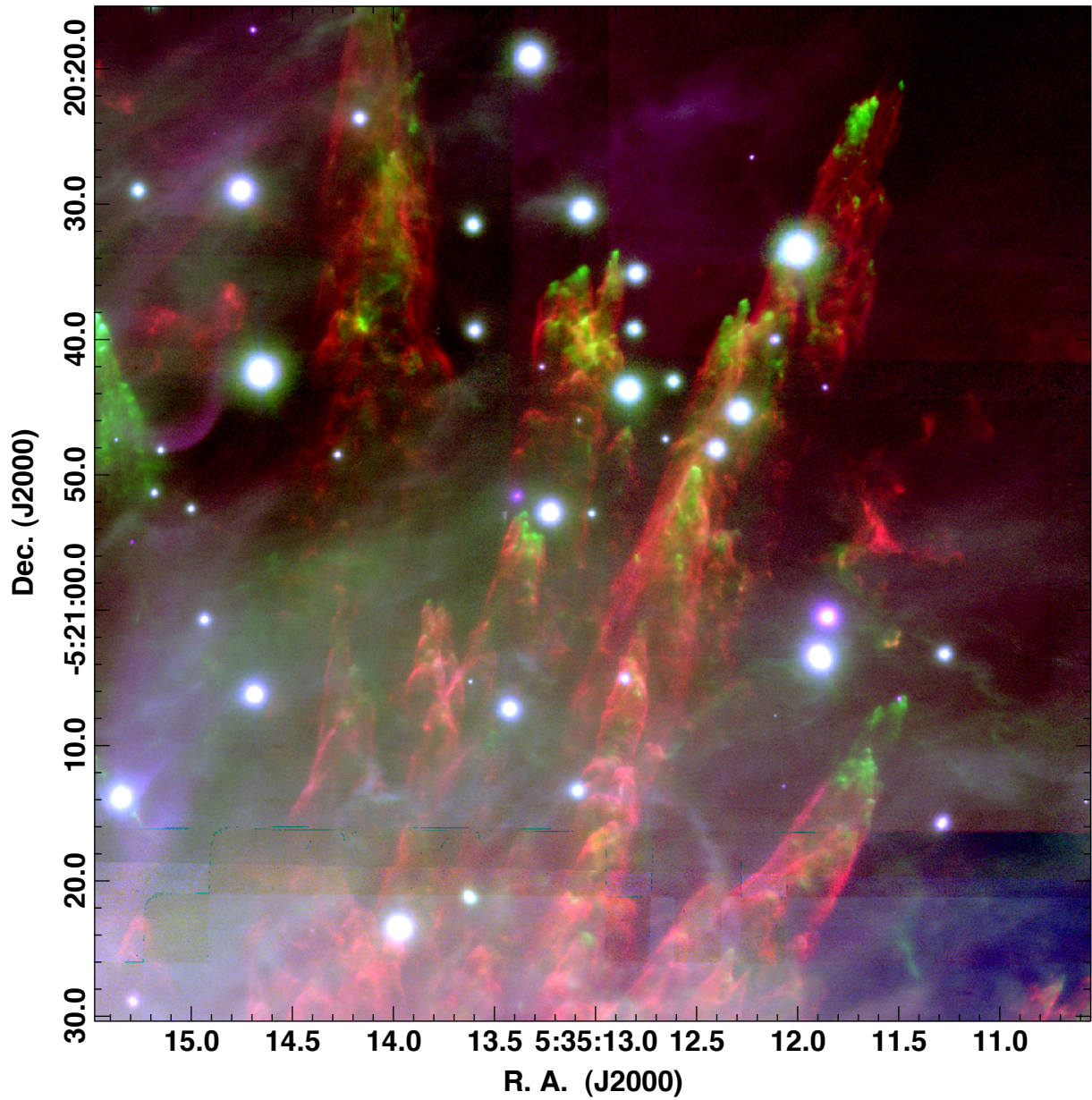


Fig. 4.— A color image showing the K_s image (blue), the $1.644 \mu\text{m}$ [FeII] image (green), and $2.122 \mu\text{m}$ H₂ (red) in the ‘H₂ fingers’ field using the GSAOI 2013 data.

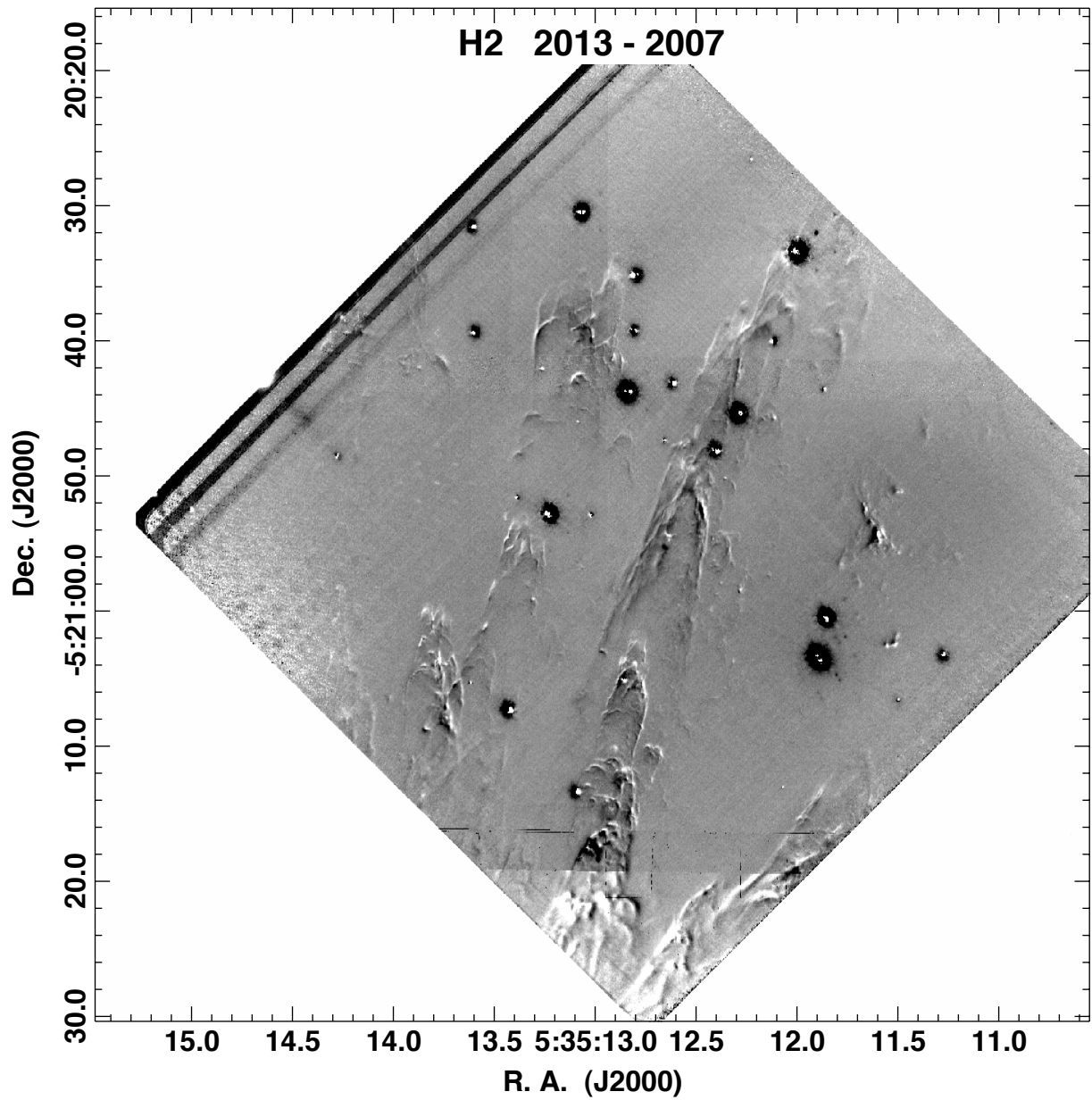


Fig. 5.— A 2.122 μm H_2 image showing proper motions in the 'H₂ fingers' field. The image shows the difference between images obtained in 2013 with Gemini S using GSAOI and in 2007 with Gemini N using NIRI.

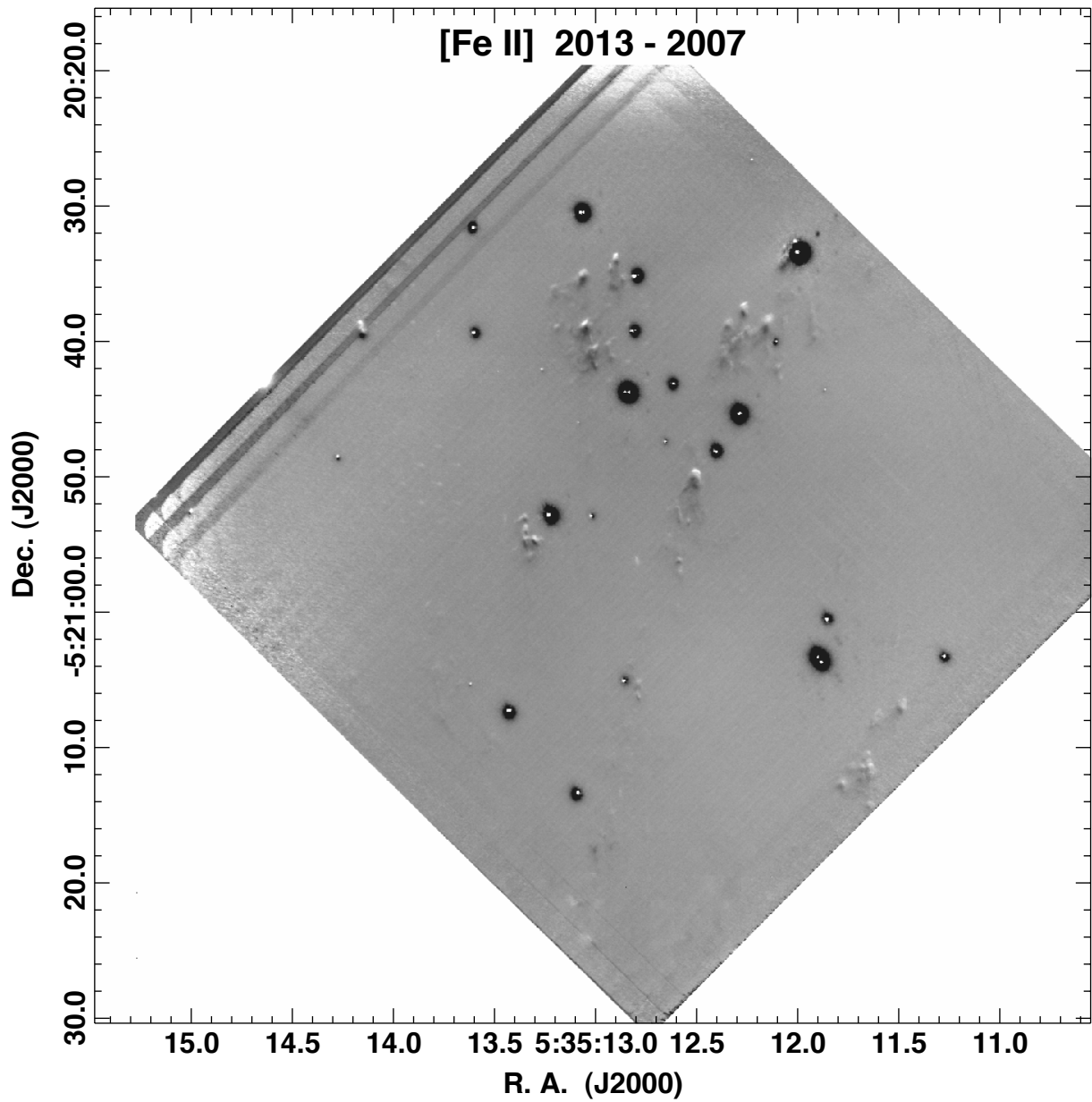


Fig. 6.— A $1.644 \mu\text{m}$ [FeII] image showing proper motions in the ‘H₂ fingers’ field. The image shows the difference between images obtained in 2013 with Gemini S using GSAOI and in 2007 with Gemini N using NIRI.

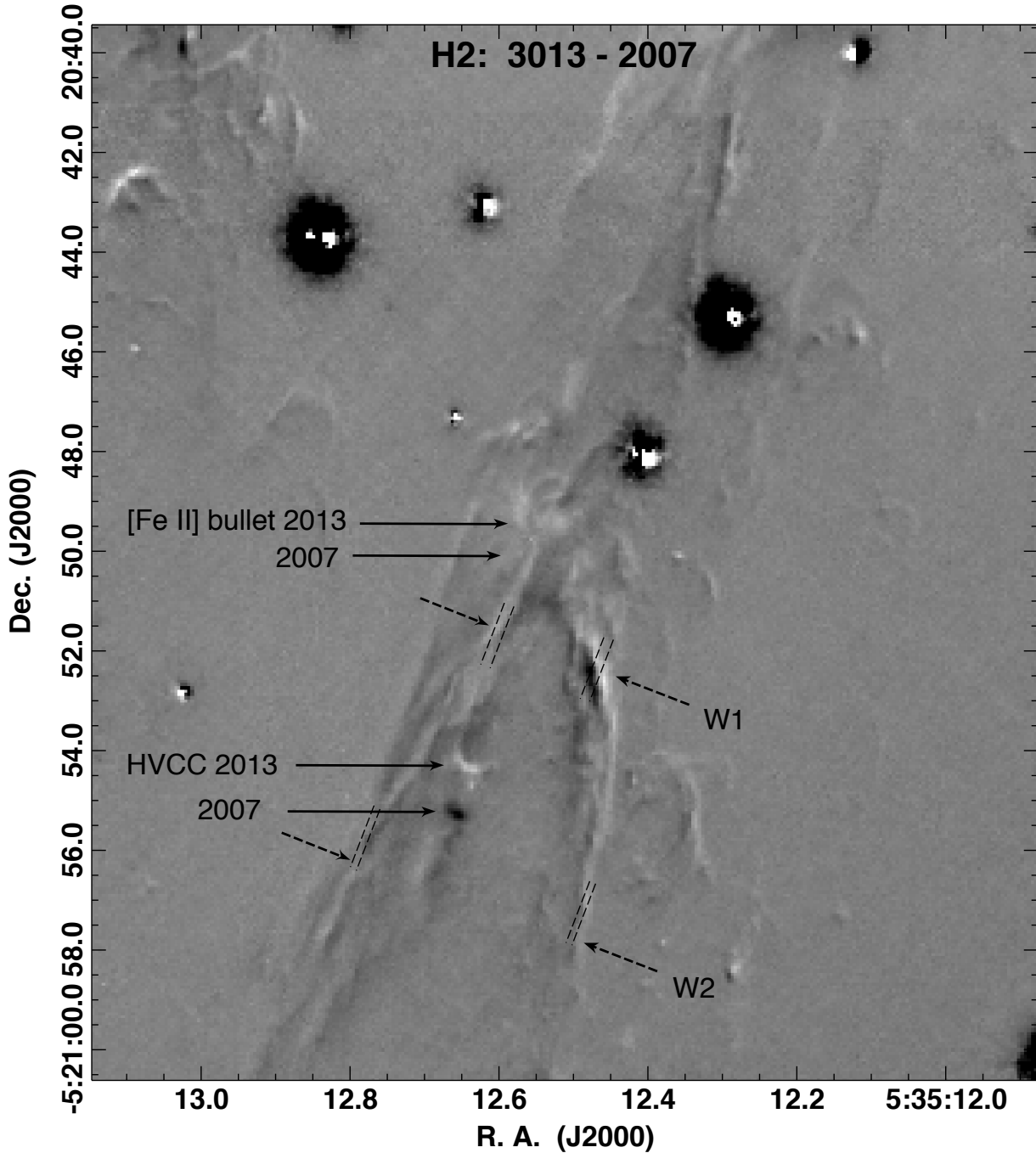


Fig. 7.— A closeup view of the main H_2 finger and the HVCC in the ‘ H_2 fingers’ field showing the difference between images obtained in 2013 with Gemini S using GSAOI and in 2007 with Gemini N using NIRI.

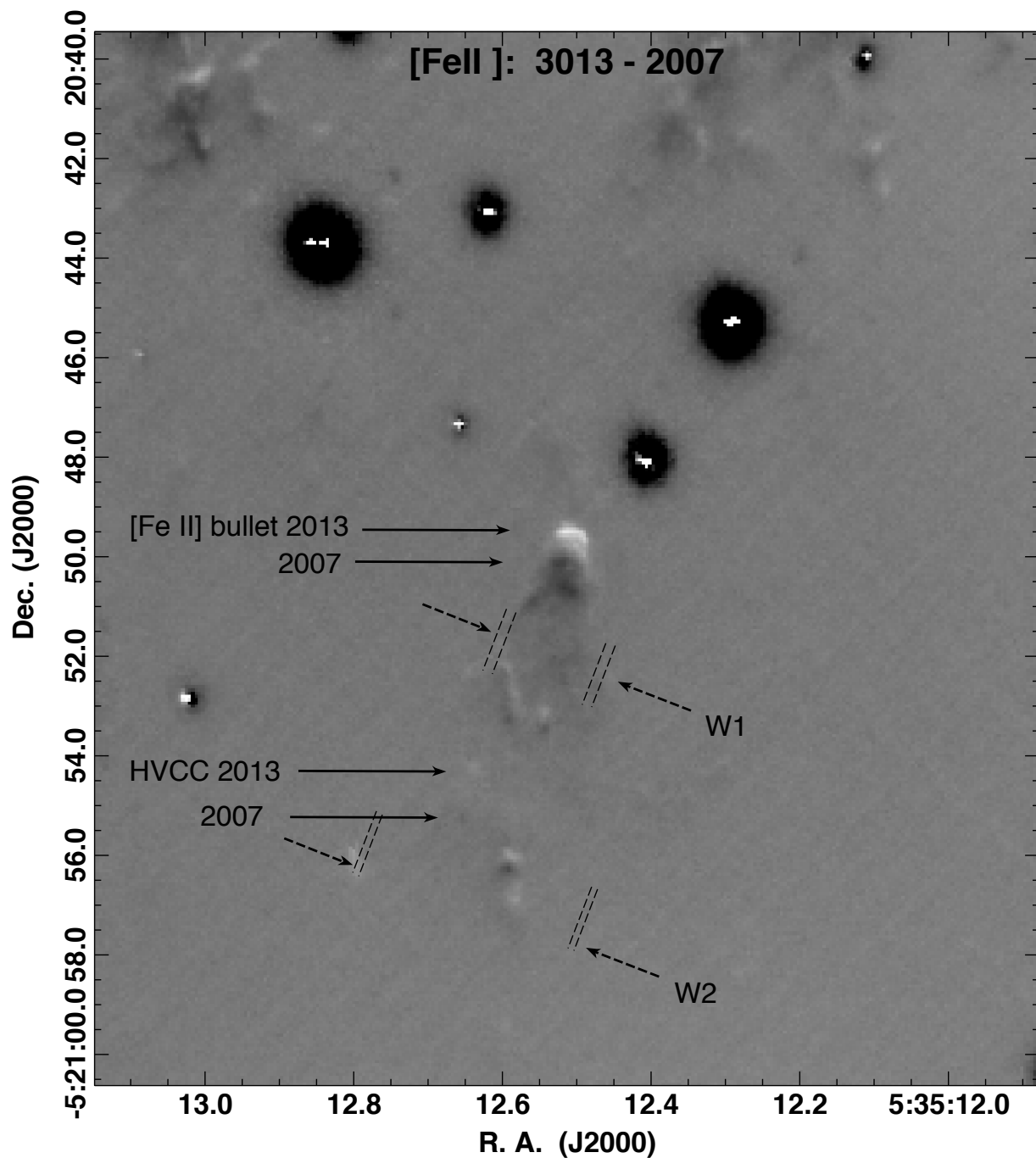


Fig. 8.— Same as Figure 7 but for [Fe II].

Table 1. Near-IR Observations of Orion OMC1

| Year | α (J2000) | δ (J2000) | Field Size | MJD | Comments |
|------|------------------|------------------|----------------------------|-------|----------------------------------|
| 2007 | 05:35:12.8 | -05:20:53 | 50'' \times 50'' at 45 ° | 54165 | H ₂ fingers; Gemini N |
| 2008 | 05:35:11.9 | -05:20:47 | 50'' \times 50'' at 45 ° | 54753 | H ₂ fingers; Gemini N |
| 2009 | 05:35:11.9 | -05:20:47 | 50'' \times 50'' at 45 ° | 55138 | H ₂ fingers; Gemini N |
| 2013 | 05:35:13.2 | -05:20:37 | 84'' \times 84'' at 0° | 56290 | OMC1 N; Gemini S |
| 2013 | 05:35:12.5 | -05:22:04 | 92'' \times 91'' at 0° | 56323 | OMC1 BN; Gemini S |
| 2013 | 05:35:17.5 | -05:22:48 | 92'' \times 91'' at 0° | | OMC1 SE; Gemini S |

Note. — Positio

Table 2. Selected OMC1 bullets and bow shocks

| Feature | α (J2000) ($05^h 35^m +$) | δ (J2000) ($-5^\circ +$) | ΔX (") | V (km s $^{-1}$) | PA ($^\circ$) | D (") | τ_{dyn} (yrs) | Comments |
|------------------|---------------------------------------|--------------------------------------|-------------------|----------------------|--------------------|----------|-----------------------|--------------------------------|
| H ₂ 1 | 12.625 | 20:55.22 | 0.88 | 297 | 346 | 100 | 662 | Fast H ₂ knot |
| 2 | 12.058 | 20:37.68 | 0.43 | 145 | 324 | 116 | 1573 | Ahead of H ₂ 1 |
| 3 | 12.270 | 20:37.82 | 0.84 | 283 | 344 | 114 | 792 | " |
| 4 | 12.351 | 20:38.84 | 0.54 | 182 | 350 | 112 | 1210 | " |
| 5 | 12.965 | 21:16.37 | 0.33 | 111 | 338 | 74 | 1310 | Cluster NE of H ₂ 1 |
| 6 | 12.989 | 21:17.73 | 0.53 | 179 | 347 | 73 | 801 | " |
| S1 | 11.532 | 21:02.24 | 0.30 | 101 | 233 | - | - | Background flow |
| S2 | 11.616 | 20:53.94 | 0.29 | 98 | 227 | - | - | " |
| S3 | 11.614 | 20:54.45 | 0.54 | 182 | 218 | - | - | " |
| W1 | 12.543 | 20:52.03 | 0.240 | 80 | - | - | 29 | Spreading H ₂ wake |
| W3 | 12.642 | 20:56.45 | 0.138 | 46 | - | - | 100 | " |
| [Fe II] 1 | 12.521 | 20:50.12 | 0.68 | 229 | 345 | 102 | 863 | [Fe II] bow |
| 2 | 12.165 | 20:39.09 | 0.81 | 273 | 345 | 116 | 835 | |
| 3 | 12.274 | 20:37.96 | 0.79 | 267 | 354 | 114 | 839 | |
| 4 | 12.353 | 20:38.94 | 0.55 | 186 | 349 | 112 | 1184 | |
| 5 | 12.898 | 20:34.12 | 0.59 | 199 | 1 | 116 | 1146 | |
| 6 | 12.932 | 20:34.87 | 0.61 | 206 | 3 | 115 | 1097 | |
| 7 | 13.066 | 20:35.39 | 0.61 | 206 | 355 | 114 | 1088 | |
| 8 | 13.052 | 20:39.01 | 0.61 | 206 | 354 | 112 | 1069 | |
| 9 | 13.010 | 20:40.81 | 0.56 | 189 | 350 | 97 | 1009 | |
| 10 | 13.308 | 20:54.78 | 0.41 | 138 | 354 | 96 | 1367 | |
| 11 | 13.386 | 20:56.16 | 0.53 | 179 | 353 | 95 | 1043 | |
| 12 | 13.354 | 20:53.14 | 0.33 | 111 | 357 | 98 | 1736 | |
| 13 | 12.592 | 20:56.23 | 0.27 | 91 | 354 | 97 | 2096 | |
| 14 | 12.795 | 21:05.50 | 0.49 | 165 | 354 | 87 | 1036 | |
| 15 | 11.502 | 21:07.20 | 0.92 | 310 | 338 | 94 | 596 | |
| 16 | 11.680 | 21:10.86 | 0.71 | 240 | 326 | 89 | 729 | |
| 17 | 11.792 | 21:12.81 | 0.41 | 138 | 329 | 86 | 1225 | |

Note. — [1]: The projected distance from the suspected point of ejection of the stars BN and source I about 500 years ago, D, is measured from J2000 = 05:35:14.35, −5:22:28.5 (Gomez et al. 2008).